Digital holographic microscopy with pure-optical spherical phase compensation

Emilio Sánchez-Ortiga,[1,*] Pietro Ferraro,[2] Manuel Martínez-Corral,[1] Genaro Saavedra,[1] and Ana Doblas[1]

[1]*3D Imaging and Display Laboratory, Department of Optics, University of Valencia, E-46100 Burjassot, Spain*
[2]*Istituto Nazionale di Ottica Applicata, 80072 Sez. Di Napoli, Italy*
**Corresponding author: Emilio.Sanchez@uv.es*

Received April 1, 2011; revised May 13, 2011; accepted May 15, 2011;
posted May 17, 2011 (Doc. ID 145197); published June 15, 2011

Telecentric architecture is proposed for circumventing, by the pure-optical method, the residual parabolic phase distortion inherent to standard configuration of digital holographic microscopy. This optical circumvention produces several important advantages. One is that there is no need for computer compensation of the parabolic phase during the phase map recovering procedure. The other is that in off-axis configuration, the spatial frequency useful domain is enlarged. The validity of the method is demonstrated by performing quantitative measurement of depth differences with high axial resolution.

OCIS codes: 180.6900, 090.1995, 110.2990.

1. INTRODUCTION

In the last decade, holography has become a very useful technique due to the development of CCD cameras that allow the recording of a digital hologram and its subsequent processing using a computer [1–4]. From a digital hologram, it is possible to retrieve numerically the complete wavefront information of a field scattered by a certain object. Specifically, one can recover plane by plane the three-dimensional (3D) information of an object by simply using a Fresnel back propagation algorithm. All these concepts can be applied, also, to recover the amplitude and phase of 3D microscope samples [5,6]. This is the case of digital holographic microscopy (DHM), which can be applied to obtain a quantitative phase-contrast image [7]. With this technique one can obtain subwavelength accuracy in the axial direction and realize the image processing that is not time consuming, so that many tasks can be carried out in real time. From these characteristics, the use of digital holography to perform quantitative phase-contrast microscopy [8,9] permits the retrieval of the quantitative phase of an object, commonly biological samples or microelectromechanical structures for the visualization of pure phase objects and cellular morphology monitoring by a dynamic differerential image contrast [10] or performing metrological measurements, respectively. It is possible to build a digital holographic microscope by simply recording a digital hologram of the wave field propagated in the imaging process of an object through a microscope objective (MO). To recover the phase information of the field scattered by the object in the typical configuration, it is necessary to remove the parabolic phase factor introduced by the MO. A lot of work has been done in the recent years [11–20] to compensate this curvature of the wavefront both numerically and physically. Many of these proposals are based on phase mask processing that requires an exact knowledge of the parameters of the system (focal lengths of the lenses, distances between the elements, etc.) or the recording of a second hologram for the subtraction of two phase maps to compensate the phase factor, which is not useful in practical cases.

In this paper, we introduce an alternative way to remove physically the phase factor working with a telecentric system so no knowledge about the parameters of the experimental setup or second hologram is necessary. This technique permits the enlargement of the spatial-frequency useful domain, since the typical circular fringe pattern is no longer present, which shifts the spatial spectrum towards low frequencies.

2. BASIC THEORY

Let us consider the case in which the monochromatic beam from a laser source is collimated and later split so that one of the resulting waves is scattered by a 3D object. Since the two split beams are mutually coherent, they have the ability of producing high-contrast interference patterns. In the forthcoming text, we will call the object beam, $O(x,y)$, to the wavefront scattered by the object, and the reference beam, $R(x,y)$, to the plane wave.

If the interference occurs at the plane of a CCD, the intensity distribution of the snapshot recorded by the camera can be written as [1–3]

$$\begin{aligned} I(x,y) &= |O(x,y)+R(x,y)|^2 \\ &= |O(x,y)|^2+|R(x,y)|^2+O^*(x,y)R(x,y) \\ &\quad +R^*(x,y)O(x,y). \end{aligned} \tag{1}$$

Here, $O^*(x,y)$ and $R^*(x,y)$ are the complex conjugate of the object and reference beams, respectively. Taking into account the pixelization of the camera, the snapshot is more rigorously described through the discrete intensity distribution

$$I_H(r,l)=\sum_{r=1}^{N_x}\sum_{l=1}^{N_y} I(r\Delta x_0, l\Delta y_0), \tag{2}$$

in which (N_x, N_y) are the number of pixels of the CCD and $(\Delta x_0, \Delta y_0)$ is the pitch.

Note now that typically the reference beam is much more intense than the object beam. Then, the factor $|O|^2$ can be neglected in Eq. (1). Besides, since the reference beam is a plane wave, $R(x, y)$ is constant so that $I(x, y)$ (or equivalently its discrete counter I_H) is in good approximation equal to $O^*R + OR^*$ over a constant background.

This snapshot constitutes the so-called digital hologram of the object. From the digital hologram, it is possible to recover a term that is proportional to the complex amplitude distribution of the object. To this end, it is necessary to get rid, first, of undesirable factors. One factor, is the DC order, $|R|^2$, which is produced in the reconstruction of an intense constant background. The other is O^*, which generates the so-called twin-image effect. The procedure for the elimination of these terms depends on the geometry of the capture setup. In particular, if the hologram is recorded employing an off-axis configuration, the terms are eliminated by applying a proper window to the Fourier transform of $I_H(r, l)$. In this form, we obtain computationally the filtered distribution $I_F(r, l)$.

To recover the object, amplitude distribution is necessary to simulate a diffraction experiment in which a plate with amplitude distribution I_F is illuminated with a plane wave that is equal to the reference beam. By application of the discrete version of the Fresnel–Kichhoff diffraction integral, we can backpropagate this amplitude distribution, and therefore calculate the complex amplitude at the object plane (OP) and its neighborhood. The equation reads [3]

$$\Gamma_d(m,n) = \frac{1}{i\lambda d}\exp\left(i\pi\lambda d\left[\left(\frac{m}{N_x\Delta x_0}\right)^2 + \left(\frac{n}{N_y\Delta y_0}\right)^2\right]\right) \times \mathrm{DFT}\left\{I_F(r\Delta x_0, l\Delta y_0)R_D(r\Delta x_0, l\Delta y_0) \times \exp\left(\frac{-ik}{2d}[(r\Delta x_0)^2 + (l\Delta y_0)^2]\right)\right\}. \quad (3)$$

In the above equation, d is the propagation distance, and R_D is the discrete version of the reference beam. Besides, m and n are integers that account for the position of the pixels in the reconstructed wavefront.

Since the discrete Fourier transform (DFT) operates between matrices with the same number of elements, $\Gamma_d(m, n)$ is a $N_x \times N_y$ matrix. Note that, since we are working in an off-axis configuration, R_D is a plane wave that propagates with a certain inclination, which is described by the wave vector $\boldsymbol{k} = (k_x, k_y)$.

The intensity distribution in the object neighborhood is obtained as [3]

$$I_d(m,n) = |\Gamma_d(m,n)|^2, \quad (4)$$

and also it is possible to recover the phase map of the field scattered by the object by applying [3]

$$\Phi_d(m,n) = \tan^{-1}\frac{\mathrm{Im}[\Gamma_d(m,n)]}{\mathrm{Re}[\Gamma_d(m,n)]}. \quad (5)$$

All these concepts, which were originally thought for application in macroscopic imaging, can also be applied to recover the amplitude and phase of a 3D microscopic sample. This is the case of DHM, in which instead of directly recording the hologram of the microscopic sample, the hologram of the intermediate, aerial image produced by the MO is recorded.

However, usual realizations of DHM fail in the fact that the aerial image is geometrically distorted and carries additional phase distortion that have to be corrected by means of numerical postprocessing.

3. IMAGING PROCESS IN DHM

Standard DHM configurations in off-axis transmission and reflection mode are based on the Mach–Zehnder interferometer and on the use of a MO with a finite conjugate ratio, as shown in Fig. 1. In the transmission mode, Fig. 1(a), the monochromatic beam coming from a fiber coupled to a laser source is collimated through a beam expander (BE). The beam is divided by a beam splitter (BS1) into the object beam and the reference beam. The object beam illuminates a thick object that is placed in the neighborhood of the OP of the MO. Finally the CCD is placed, perpendicular to the object beam, at a certain distance of the image plane (IP). On the other hand, a second beam splitter (BS2) forming a certain angle with the direction of the object beam allows the interference in an off-axis configuration between the object beam and the tilted reference beam at the CCD plane. Therefore, the CCD captures a hologram, which is, basically, the interference between the defocused image of the microscopic sample and the reference beam.

The main difference between the transmission mode and the reflection mode [Fig. 1(b)], is that in the later, the MO is used to illuminate both the sample and collect the scattered light. As shown in Fig. 1, for recording the digital hologram, the object is illuminated with a plane wave. For this reason, the CCD of the DHM arrives at the wavefront that includes not only the phase information of the defocused image, $\Phi^d_{\mathrm{ob}}(x, y)$, but also a spherical phase factor whose radius of curvature μ is just the distance from the image principal plane of the MO to the CCD.

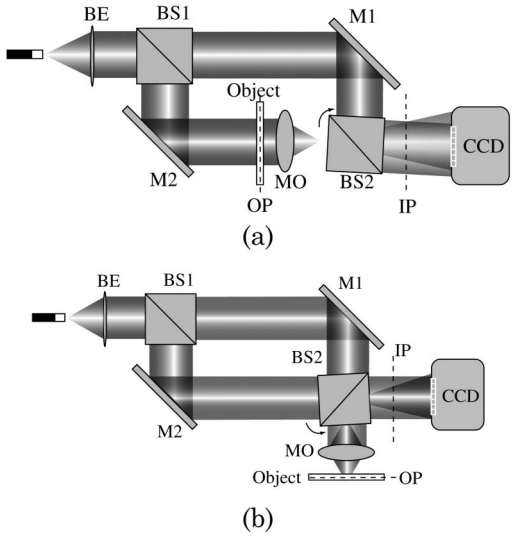

Fig. 1. Typical scheme based on Mach–Zehnder interferometer for off-axis DHM in (a) transmission mode and (b) reflection mode.

In the paraxial approximation, this phase factor can be written as [11]

$$\Phi(x,y)=\frac{ik}{2\mu}(x^2+y^2)+\Phi_{\mathrm{ob}}^{d}(x,y). \tag{6}$$

The interference between the object wavefront and the reference wavefront gives rise to a digital hologram in which, superimposed to the object information, appears a pattern similar to the well-known Newton ring. This pattern is due to the interference between the spherical phase factor and the reference beam.

As a simple proof of the existence of this fringe pattern, we performed a preliminary DHM experiment. The scheme of our experimental setup was similar to the one shown in Fig. 1(a). In particular, we used the monochromatic beam emitted by a He-Ne laser for illumination (632.8 nm). For the BE, we use a converging lens of $f_E = 100$ mm. For the imaging lens, we used a $10\times$ MO ($f_{\mathrm{ob}} = 20$ mm) with NA $= 0.45$. Finally, for matrix sensor, we used a CCD with 765×578 pixels of 11 μm placed at 31 cm of the IP. With this instrument, we recorded a digital hologram in absence of an object. The hologram recorded with in-line and off-axis configuration is shown in Figs. 2(a) and 2(b), respectively. As expected, we can see the typical interferogram due to the interference between the spherical and plane waves. In addition, Fig. 2(c) shows the retrieved phase map of the reconstructed wavefront clearly affected by a spherical phase factor.

This superimposed ring pattern increases the complexity of the numerical reconstruction process and can produce important distortion in the reconstructed phase maps. Thus, several techniques have been proposed for the compensation of the residual spherical phase factor. One way to remove it is with a postprocessing numerical method by means of a phase mask that matches the phase of the residual factor [11–15]. Other techniques are based on the physical introduction of the same curvature in [16–18]: by wavefront folding [19] and by self-reference interferometry [20] for application in microfluidics or in the use of a single cube beam splitter in a nonconventional DHM configuration [21]. The use of a tube lens (TL) has been proposed for the nonholographic measurement of the focal length of microlenses [22].

4. SUPPRESSION OF THE PHASE DISTORTION BY THE PURE-OPTICAL METHOD

What we propose here is the simplest, almost trivial, solution to the problem of the residual phase factor. Specifically, we propose an optical arrangement, for the capture of the hologram, which does not produce the spherical phase factor. The solution then consists of the use of a telecentric arrangement. Indeed, the use of telecentric arrangements in DHM is facilitated by the fact that modern MO are usually designed for a infinite conjugate ratio [23]. For this reason, a second lens (the TL) of higher focal length and smaller NA, is used to provide the intermediate, floating image in the neighborhood of its back focal plane. The telecentric system (Fig. 3) formed by the MO and the TL in an afocal ($F'_{\mathrm{ob}} \equiv F'_L$) configuration produces a 3D amplitude distribution in the image space which is, basically, a scaled copy of the original object but slightly blurred due to the convolution with the point-spread function

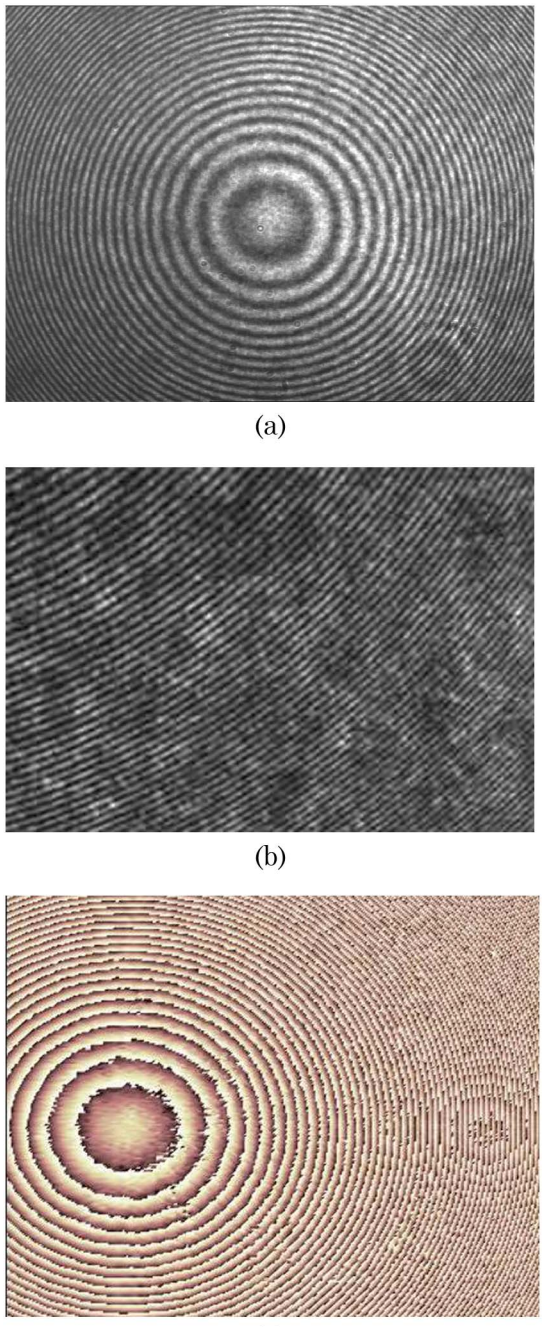

(a) (b) (c)

Fig. 2. (Color online) Hologram obtained with a standard, nontelecentric, DHM architecture in absence of an object with (a) in-line configuration and (b) off-axis configuration. (c) Retrieved phase map for the hologram in (b), showing wrapped-spherical phase-factor.

(PSF) of the telecentric system. If we consider the imaging process through this telecentric system of a volume object with amplitude transmittance, namely $U_o(x,y,z)$, then the amplitude distribution in the image space will be [24]

$$U'_o(x,y,z)=\frac{1}{M^2}U_o\left(\frac{x}{M},\frac{y}{M},\frac{z}{M^2}\right)\otimes_3 h(x,y,z), \tag{7}$$

where $\otimes_3$ is the 3D convolution, $M=-f_L/f_{\mathrm{ob}}$ is the magnification of the telecentric arrangement, and $h(x,y,z)$ is the PSF of the telecentric system.

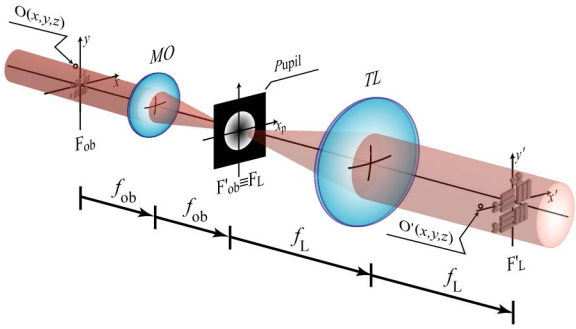

Fig. 3. (Color online) Schematic of a telecentric microscope.

Note that the distance between the MO aperture stop and the TL is the same for different MOs. In fact, infinite conjugate MOs are designed for convenient correction of aberrations provided that the object is near the MO front focal plane, and therefore the image is near the TL back focal plane.

As we can see, no parabolic phase factor is introduced by the optical elements. With this configuration, the only two differences between recording the object itself or recording its image is the size of the hologram area and the frequency loss due to the PSF of the objective. As the recording of a hologram in digital holographic microscopy is, basically, the recording of the information contained in the propagated wave field of the image of an object, the process with this telecentric arrangement can be seen like illuminating this "magnified and blurred copy of the object" with a plane wave and perform the interference with a plane reference wave coherent with the first one. By this, the amplitude and phase reconstruction can be done with the typical methods developed in digital holography.

As is well-known, the retrieved phase is defined in mod2π so that it has to be unwrapped to suppress the phase jumps [25,26]. In the simplest case of a dry MO and a object with constant refraction index n, to retrieve 3D information in terms of depth measurement from the unwrapped tilt-compensated phase map, namely $\bar{\Phi}(x,y)$, it is possible to apply the next relationship [6]

$$\bar{\Phi}(x,y) = \frac{2\pi n}{\lambda} t_I(x,y), \tag{8}$$

where $t_I(x,y)$ is the thickness of the image of the sample. To obtain a real measurement for quantitative phase, the magnification factor M, introduced by the telecentric system, has to be taken into account so it can be seen in Eq. (6). The relationship between the image and object spaces is

$$t_o(x,y) = \frac{t_I(x,y)}{M^2}, \tag{9}$$

where $t_o(x,y)$ is the quantitative value of the depth in the object space.

Furthermore, with this setup, all transversal planes are affected by the same scale factor so an identical zone of the object will be recorded independently of the CCD position.

5. EXPERIMENTAL VERIFICATION

The schemes of the telecentric DHM working in transmission and reflection mode are shown in Fig. 4. In the particular case

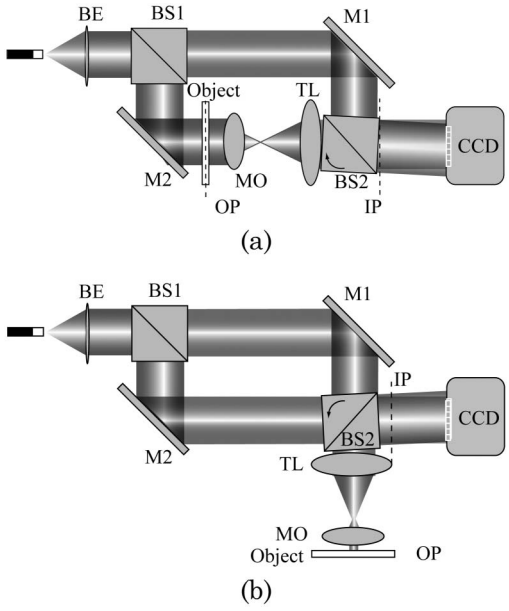

Fig. 4. Telecentric configuration for off-axis DHM in (a) transmission mode and (b) reflection mode.

of the transmission DHM, Fig. 4(a), we have simply added, in the adequate position, a TL with focal length $f_L = 150\,\text{mm}$. The focal length of the objective is still $f_{\text{ob}} = 20\,\text{mm}$, and therefore the scale factor $M = -7.5$. Naturally, this value of M will be used for the calculation of depth distances. To show the utility of this arrangement we have performed, as in the previous Section, a preliminary experiment is done in which we record a digital hologram in absence of an object.

The reference beam was slightly tilted so that $k_x = 0.53$ and $k_y = 0.42$. The recorded hologram is shown in Fig. 5. As expected, the fringe pattern is the typical interferogram due to the interference between tilted plane waves. Naturally, no radial fringes appear. This is the proof that no residual spherical phase factor is created and, therefore, there is no need for developing techniques for its suppression.

Note, however, that although in Fig. 5 is it easy to see that the fringes are not radial, in the case of other experiment in which the density of the fringes were much more higher, this conclusion would not be so easy. Then to make sure that the objective and the TL are truly arranged in telecentric manner (and therefore the fringes are really straight), a good strategy is to inspect the Fourier transform of the recorded hologram.

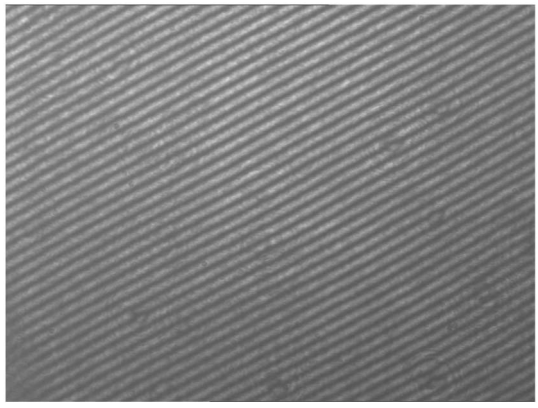

Fig. 5. Hologram obtained with an off-axis, telecentric DHM in the absence of an object.

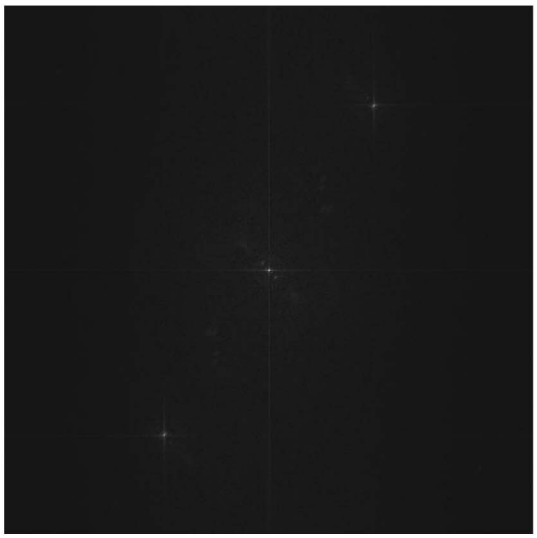

(a)

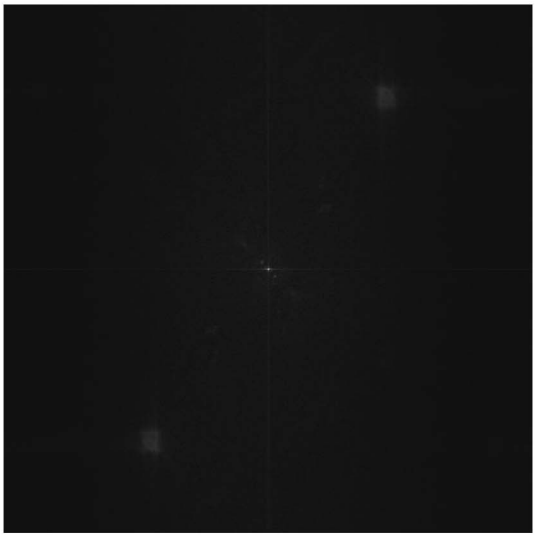

(b)

Fig. 6. Fourier transform of the recorded hologram in absence of an object for the case in which the arrangement is (a) telecentric and (b) nontelecentric. The effect of the variation of the TL position in the spectrum can be appreciated in Media 1.

Note that in absence of the residual phase factor, such a Fourier transform is composed, basically, by three deltas (in practice three narrow and sharp light dots). However, when the residual spherical phase is present, the Fourier transform is composed by the same three deltas, but spread. To illustrate this, by using the same experimental setup as in Fig. 5, we recorded different holograms after performing a gradual variation of the distance between the objective and the TL. In Fig. 6(a), we show the three delta spectrum, which was obtained at the telecentric distance. In Fig. 6(b), we show the spectrum obtained when the arrangement was not telecentric. Finally, we have composed a movie (Media 1) in which the frames are the spectra calculated for varying distances of the arrangement.

As the second part of this preliminary experiment, we have suppressed the DC term and the twin image by applying a circular filter rounding the real-image term in the Fourier domain

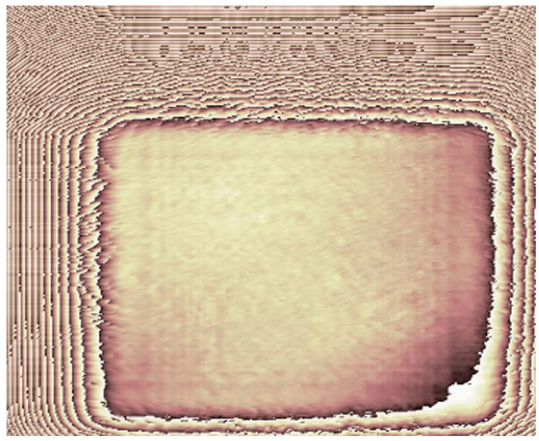

(a)

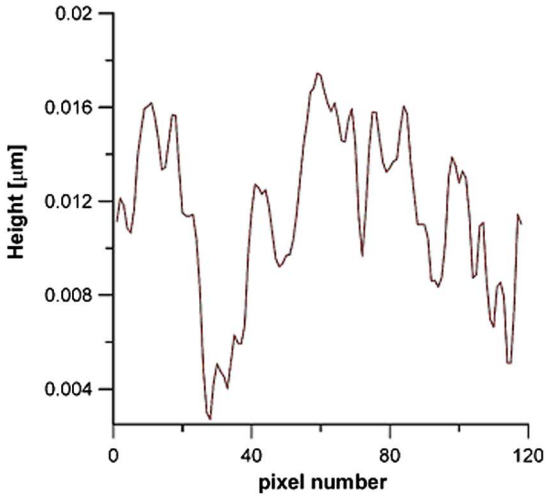

(b)

Fig. 7. (Color online) (a) Direct phase of the reconstructed hologram. (b) Roughness parameters of the center zone of the quantitative phase extracted from the red line profile in (a).

[27]. Then, we have applied the back propagation algorithm (Eq. (3)) and obtained the phase map that is shown in Fig. 7(a). Also, a profile of the quantitative phase in shown in Fig. 7(b). As we can see, there is no trace of the spherical factor. Besides, the later plot serves as proof of the accurateness of this DHM for the quantitative evaluation of the phase differences. In particular, we see that in the surface, in pure theory it should be flat in phase, we have measured very small variations around the mean value. The standard deviation of the values shown in Fig. 7(b) is $\sigma = 0.008\,\mu$m. So, we can affirm that the telecentric DHM can measure depth distance (or equivalently phase differs) with precision of some nanometers.

6. QUANTITATIVE MEASUREMENT OF PHASE DIFFERENCES

Once we have demonstrated the utility of the telecentric DHM, next we perform some experiments in which we measure, with high precision, some axial distances.

In our first experiment, we used an USAF 1951 resolution test target as the object. Such a test is composed by strips of

evaporated chromium on soda-line glass. Typically, the height of the chrome deposition is 50 nm [28]. Then, we placed the object in the focal plane of the MO of telecentric DHM, working this time in reflection mode, and recorded the digital hologram. For this capture, the CCD was placed at a distance of 230 mm from the IP.

In Fig. 8, we show the recorded digital hologram as well as the intensity distribution at the OP. Note that the hologram corresponds to the 4-3 test group, which has 22.6 lines per mm.

But the important part of our experiment is the measurement of depth distances with nanometer precision. In this sense, in Fig. 9, we have plotted the unwrapped phase map obtained from the reconstructed wavefront. The measured profile of the 4-3 group is shown in Fig. 10.

In a second example, the object was a diffractive Fresnel lens with two values for the phase. The direct tilt compensated phase map obtained in the focus plane and the quantitative phase are shown in Fig. 11. The hologram was recorded by means of an off-axis transmission mode. The CCD was placed at 320 mm from the IP, and the size of the quantitative phase image is 220×240 pixels.

In order to evaluate the accurateness of the telecentric DHM for the quantitative measurement of phase variations, we measured the depth of the grooves of the zone plate with a profilometer (Dektak 6 M), whose depth resolution is of 16 nm. In Fig. 12, we have plotted the grooves depth along one period, measured with the profilometer (red curve) and with the telecentric DHM (blue curve).

From Fig. 12, we find a very good agreement between the measurements of both instruments. This confirms the validity of telecentric DHM for accurate quantitative evaluation of phase variations of 3D microscopic samples. Note that although the lateral resolution of the profilometer is much higher than the one of the telecentric DHM [29], the accuracy of both techniques in the evaluation of the depth of phase steps is similar.

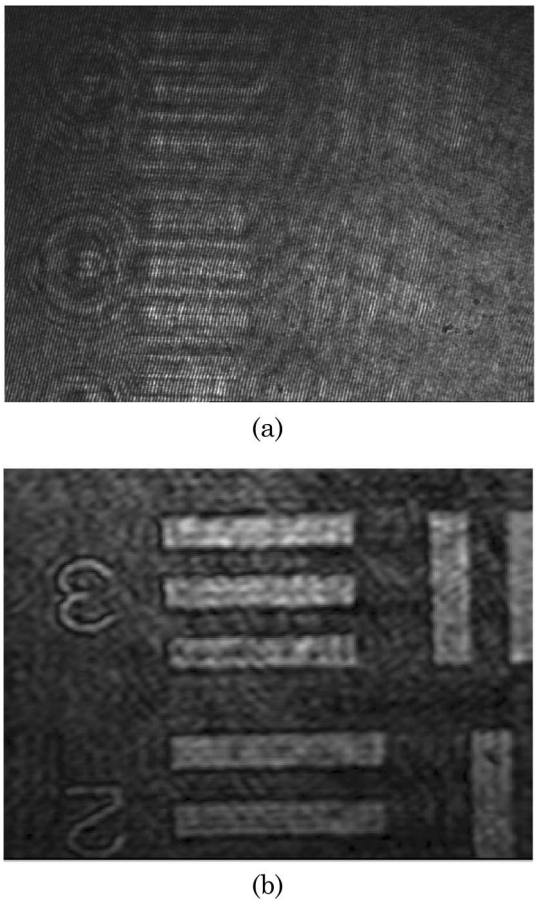

Fig. 8. (a) Recorded hologram. (b) Reconstruction of the object intensity distribution.

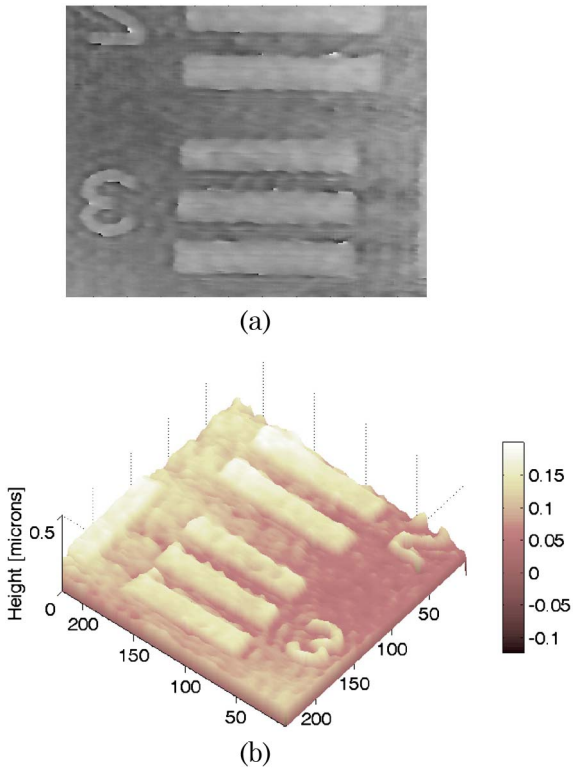

Fig. 9. (Color online) Phase reconstruction of a test USAF 1951 in an off-axis reflection mode. (a) Phase map. (b) Quantitative phase.

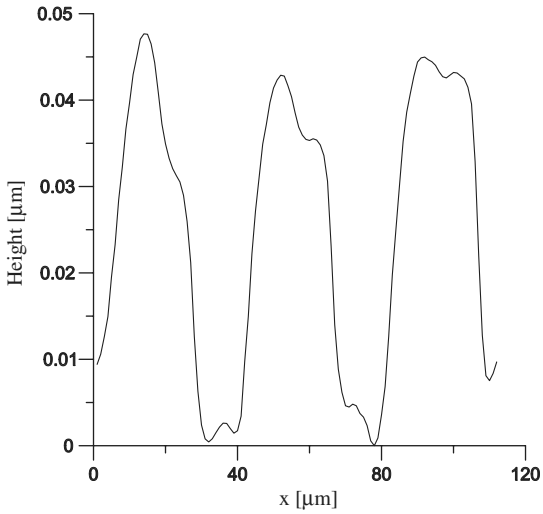

Fig. 10. Profile of the reconstruction in Fig. 9. The structure corresponds to a 4-3 group.

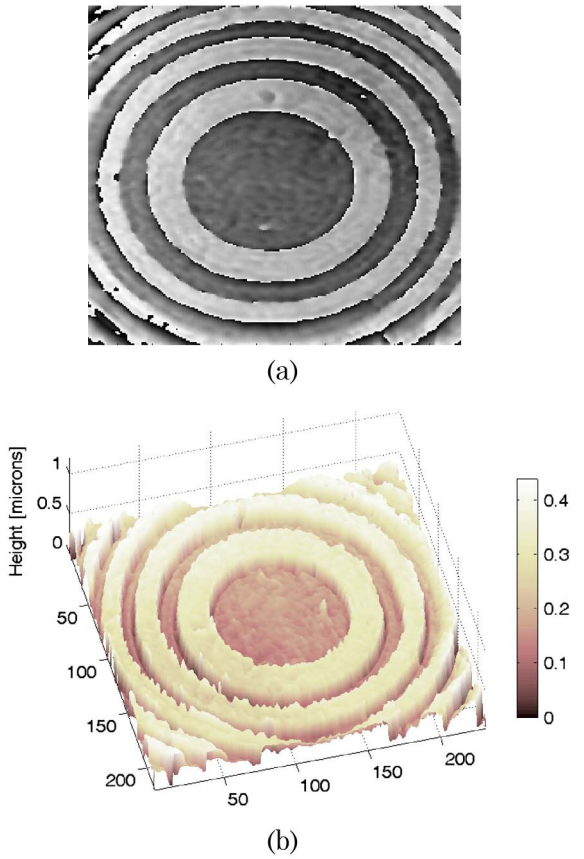

Fig. 11. (Color online) Measured phase reconstruction of a bivaluated Fresnel lens obtained by DHM in off-axis transmission mode. (a) Phase map. (b) Quantitative phase.

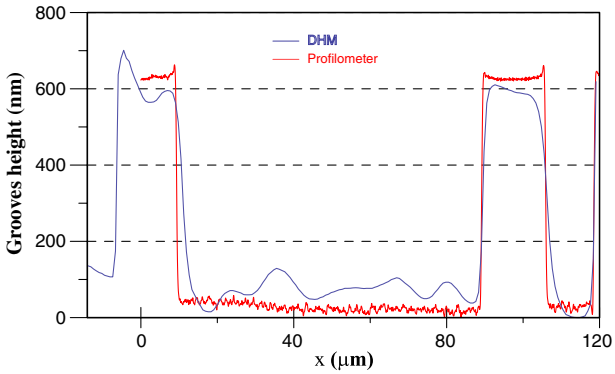

Fig. 12. (Color online) Measured profile of the Fresnel lens.

7. CONCLUSIONS

In this paper, we have presented a new scheme for DHM which includes a TL in telecentric configuration with the MO. As a consequence, the object beam (in absence of sample) becomes a plane wave with no phase distortion in the imaging process, so the phase factor introduced by the objective lens is physically corrected. Besides, this configuration provides a hologram in which the recording zone is independent of the CCD position. We demonstrate the applicability for quantitative phase imaging in off-axis transmission and reflection mode. This configuration can be applied for recording inline holograms taking in account all the consideration for the off-axis case.

ACKNOWLEDGMENTS

This work was supported in part by the Plan Nacional I+D+I under grant FIS2009-9135 and also by Generalitat Valenciana under grant PROMETEO2009-077.

REFERENCES

1. U. Schnars and W. Jüptner, "Direct recording of holograms by a CCD target and numerical reconstruction," Appl. Opt. **33**, 179–181 (1994).
2. U. Schnars, "Direct phase determination in hologram interferometry with use of digitally recorded holograms," J. Opt. Soc. Am. A **11**, 2011–2015 (1994).
3. E. Cuche, P. Marquet, and C. Depeursinge, "Simultaneous amplitude-contrast and quantitative phase-contrast microscopy by numerical reconstruction of Fresnel off-axis holograms," Appl. Opt. **38**, 6994–7001 (1999).
4. S. Grilli, P. Ferraro, S. De Nicola, A. Finizio, G. Pierattini, and R. Meucci, "Whole optical wavefields reconstruction by digital holography," Opt. Express **9**, 294–302 (2001).
5. D. Gabor, "A new microscopic principle," Nature **161**, 777–778 (1948).
6. P. Marquet, B. Rappaz, P. J. Magistretti, E. Cuche, Y. Emery, T. Colomb, and C. Depeursinge, "Digital holographic microscopy: a non-invasive contrast imaging technique allowing quantitative visualization of living cells with subwavelenght axial accuracy," Opt. Lett. **30**, 468–471 (2005).
7. E. Cuche, F. Bevilacqua, and C. Depeursinge, "Digital holography for quantitative phase-contrast imaging," Opt. Lett. **24**, 291–293 (1999).
8. N. T. Shaked, M. T. Rinehart, and A. Wax, "Dual-interference-channel quantitative-phase microscopy of live cell dynamics," Opt. Lett. **34**, 767–770 (2009).
9. G. Popescu, L. P. Deflores, J. C. Vaughan, K. Badizadegan, H. Iwai, R. R. Dasari, and M. S. Feld, "Fourier phase microscopy for investigation of biological structures and dynamics," Opt. Lett. **29**, 2503–2506 (2004).
10. L. Miccio, A. Finizio, R. Puglisi, D. Balduzzi, A. Galli, and P. Ferraro, "Dynamic DIC by digital holography microscopy for enhancing phase-contrast visualization," Biomed. Opt. Express **2**, 331–344 (2011).
11. P. Ferraro, S. De Nicola, A. Finizio, C. Coppola, S. Grilli, C. Magro, and G. Pierattini, "Compensation of the inherent wave front curvature in digital holographic coherent microscopy for quantitative phase-contrast imaging," Appl. Opt. **42**, 1938–1946 (2003).
12. T. Colomb, F. Montfort, J. Kühn, N. Aspert, E. Cuche, A. Marian, F. Charrière, S. Bourquin, P. Marquet, and C. Depeursinge, "Numerical parametric lens for shifting, magnification, and complete compensation in digital microscopy," J. Opt. Soc. Am. A **23**, 3177–3190 (2006).
13. P. Ferraro, D. Alferi, S. De Nicola, L. De Petrocellis, A. Finizio, and G. Pierattini, "Quantitative phase-contrast microscopy by a lateral shear approach to digital holographic image reconstruction," Opt. Lett. **31**, 1405–1407 (2006).
14. F. Montfort, F. Charrière, T. Colomb, E. Cuche, P. Marquet, and C. Depeursinge, "Purely numerical compensation for microscope objective phase curvature in digital holographic microscopy: influence of digital phase mask position," J. Opt. Soc. Am. A **23**, 2944–2953 (2006).
15. Z. W. Zhou, Y. Yingjie, and A. Asundi, "Study on aberration suppresing methods in digital micro-holography," Opt. Lasers Eng. **47**, 264–270 (2009).
16. C. J. Mann, L. Yu, C. Lo, and M. K. Kim, "High-resolution quantitative phase-contrast microscopy by digital holography," Opt. Express **13**, 8693–8698 (2005).
17. T. Ikeda, G. Popescu, R. R. Dasari, and M. S. Feld, "Hilbert phase microscopy for inversting fast dynamics in trnsparent systems," Opt. Lett. **30**, 1165–1167 (2005).
18. T. Colomb, J. Kühn, F. Charière, and C. Depeursinge, "Total aberrations compensation in digital holographic microscopy

with a reference conjugated hologram," Opt. Express **14**, 4300–4306 (2006).
19. G. Coppola, G. Di Caprio, M. Gioffré, R. Puglisi, D. Balduzzi, A. Galli, L. Miccio, M. Paturzo, S. Grilli, A. Finizio, and P. Ferraro, "Digital self-referencing quantitative phase microscopy by wavefront folding in holographic image reconstruction," Opt. Lett. **35**, 3390–3392 (2010).
20. J. Jang, C. Y. Bae, J.-K. Park, and J. C. Ye, "Self-reference quantitative phase microscopy for microfluidic devices," Opt. Lett. **35**, 514–516 (2010).
21. Q. Weijan, Y. Yingjie, C. O. Choo, and A. Asundi, "Digital holographic microscopy with physical phase compensation," Opt. Lett. **34**, 1276–1279 (2009).
22. T. Kozacki, M. Józwik, and R. Józwicki, "Determination of optical field generated by using digital holography," Opto-Electron. Rev. **17**, 211–216 (2009).
23. R. Juskaitis, "Characterizing high-NA microscope objective lenses," in *Optical Imaging and Microscopy: Techniques and Advanced Systems*, P. Török and F. J. Kao, eds. (Springer, 2003), pp. 21–43.
24. M. Martínez-Corral and G. Saavedra, "The resolution challenge in 3D optical microscopy," Prog. Opt. **53**, 1–67 (2009).
25. R. M. Goldstein, H. A. Zebker, and C. Werner, "Satellite radar interferometry: two-dimensional phase unwrapping," Radio Sci. **23**, 713–720 (1988).
26. L. Aiello, D. Riccio, P. Ferraro, S. Grillo, L. Sansone, G. Coppola, S. De Nicola, and A. Finizio, "Green's formulation for robust phase unwrapping in digital holography," Opt. Lasers Eng. **45**, 750–755 (2007).
27. E. Cuche, P. Marquet, and C. Depeursinge, "Spatial filtering for zero-order and twin-image elimination in digital off-axis holography," Appl. Opt. **39**, 4070–4075 (2000).
28. J. Kühn, E. Cuche, Y. Emery, T. Coulomb, F. Charrière, F. Monfort, M. Botkine, N. Aspert, and C. Depeursinge, "Measurements of corner cubes microstructures by high-magnification digital holographic microscopy," Proc. SPIE **6188**, 618804 (2006).
29. P. Picart and J. Leval, "General theoretical formulation of image formation in digital Fresnel holography," J. Opt. Soc. Am. **25**, 1744–1761 (2008).